Applied Catalysis B: Environmental 241 (2019) 367–374

Contents lists available at ScienceDirect

Applied Catalysis B: Environmental

journal homepage: www.elsevier.com/locate/apcatb

Photo-Fenton degradation of phenol by CdS/rGO/Fe^{2+} at natural pH with *in situ*-generated H_2O_2

Zhenying Jiang[a], Lingzhi Wang[a], Juying Lei[b,c,**], Yongdi Liu[b,c], Jinlong Zhang[a,*]

[a] Key Lab for Advanced Materials and Institute of Fine Chemicals, East China University of Science and Technology, 130 Meilong Road, Shanghai 200237, PR China
[b] State Environmental Protection Key Laboratory of Environmental Risk Assessment and Control on Chemical Process, School of Resources and Environmental Engineering, East China University of Science and Technology, 130 Meilong Road, Shanghai 200237, PR China
[c] Shanghai Institute of Pollution Control and Ecological Security, Shanghai 200092, PR China

ARTICLE INFO

Keywords:
In situ generation of H_2O_2
Fenton
Degradation
Natural pH
Phenol

ABSTRACT

The application of photo-Fenton process is restricted by the acidic pH and additional hydrogen peroxide (H_2O_2). In order to overcome these drawbacks, a photo-Fenton system of CdS/rGO/Fe^{2+} which can perform at natural pH with *in situ*-generated H_2O_2 has been successfully developed. Highly efficient photo-Fenton degradation of phenol was achieved under the visible light irradiation *via* the CdS/rGO/Fe^{2+} system. Experimental results showed that phenol could be degraded completely in 1 h at natural pH. The plentiful *in situ* generation of H_2O_2 was further proved to act as an important role in phenol degradation with the addition of Fe^{2+}. The advantages of degradation at natural pH with *in situ*-generated H_2O_2 can provide a new prospective to the environmental-friendly Fenton process.

1. Introduction

Water pollution has become more serious than before due to the excessive sewage disposal, especially with some toxic organic pollutants. It has detrimental effects not only on the environment but also on human health. For wastewater treatment, the photo-Fenton process has been well regarded as an efficient alternative process because of its superior efficiency and technical feasibility [1–3]. Photo-Fenton process starts with the classical reaction as shown in Eq. (1) to generate $HO^{\cdot}$. Simultaneously, with the presence of light illumination, Fe^{3+} can be reduced (Eq. (2)) to be utilized circularly [4–6]. Furthermore, iron is highly abundant on earth and non-toxic, while, H_2O_2 is environmentally benign. Therefore, photo-Fenton process has still been one of the most efficient and promising processes for wastewater treatment [7–9].

$$Fe^{2+} + H_2O_2 \rightarrow Fe^{3+} + HO^{-} + HO^{\cdot} \quad (1)$$

$$Fe^{3+} + H_2O + h\nu \rightarrow Fe^{2+} + HO^{\cdot} + H^{+} \quad (2)$$

However, the application of photo-Fenton process has several drawbacks including the acidic pH values and additional H_2O_2. A strict pH control can ensure that Fe^{2+} and Fe^{3+} species exert their catalytic role and maximize the concentration of photoactive species, but with requiring the addition of acidifying reagents, the final neutralization will has relevant environmental and economic disadvantages [10–12]. Yong Liu [13] et al. developed a Fenton-like catalyst Zn-Fe-CNTs, which showed excellent degradation of sulfamethoxazole with initial pH = 1.5. However, the concentration of Zn^{2+} increased rapidly with pH increased and it possibly led to another environmental problem. Therefore, the photo-Fenton process at natural pH aroused great interest. Another drawback is additional H_2O_2. The transportation and storage of concentrated H_2O_2 is challenging and very costly [14]. In addition, present manufacturing process of H_2O_2 is not environmentally benign because it requires costly hydrogen gas, toxic organic solvents and high energy inputs [15,16]. Fabrication and design of efficient photo-Fenton system that avoid the introduction of H_2O_2 has become an active research front [17]. One of the methods to overcome the excessive use of H_2O_2 is the *in situ* generation of H_2O_2 [18,19]. Mohammad [20] et al. reported *in situ* generation of H_2O_2 from formic acid and oxygen for degradation of phenol on an alumina supported palladium catalyst. However, the introduction of noble metal is greatly limited in practical application due to its high economic costs. Gun-hee Moon [21] et al. demonstrated a noble metal-free catalyst, WO_3/g-C_3N_4, displaying a highly enhanced activity for efficient oxidation of As

* Corresponding author at: Key Lab for Advanced Materials and Institute of Fine Chemicals, East China University of Science and Technology, 130 Meilong Road, Shanghai 200237, PR China.
** Corresponding author at: Shanghai Institute of Pollution Control and Ecological Security, Shanghai 200092, PR China.
E-mail addresses: leijuying@ecust.edu.cn (J. Lei), jlzhang@ecust.edu.cn (J. Zhang).

https://doi.org/10.1016/j.apcatb.2018.09.049
Received 30 July 2018; Received in revised form 14 September 2018; Accepted 16 September 2018
Available online 17 September 2018
0926-3373/

(III) with *in situ*-generated H_2O_2 as a Fenton agent. Nonetheless, the vast addition of ferric ions needed lower pH to facilitate the regenerative cycle of Fe^{3+} to Fe^{2+}, which led to extra cost. Hence, a photo-Fenton degradation at natural pH with *in situ*-generated H_2O_2 is of great importance.

In this study, a CdS/reduced graphene oxide (rGO) composite has been synthesized, a photo-Fenton system of CdS/rGO/Fe^{2+} with *in situ*-generated H_2O_2 was constructed. In this system, the CdS/rGO composite photocatalytically generated H_2O_2 with a rate of 580.68 μmol/L, which was then utilized by Fe^{2+} to form hydroxyl radicals. This system demonstrated a superior activity for degradation of organic pollutants represented by phenol. In addition, different from the tradition Fenton, this system can work without adjusting pH values and be conducted at natural pH. Our results presented here open a new avenue for developing a novel route beyond tradition Fenton process.

2. Experimental sections

2.1. Materials

All chemical reagents used in this work including cadmium acetate ($Cd(CH_3CO_2)_2{\cdot}2H_2O$), thiourea ($H_2NCSHN_2$), 5,5-Dimethyl-1-pyrroline-*N*-oxide (DMPO), benzoic acid (BA), potassium permanganate ($KMnO_4$), sodium nitrate ($NaNO_3$), sulfuric acid (H_2SO_4), hydrogen peroxide (H_2O_2), hydrochloric acid (HCl) and graphite powder were purchased from Aladdin, China.

2.2. Preparation of graphene oxide

Graphene Oxide (GO) was synthesized by a modified Hummer's method [22]. In a typical procedure, 2.0 g of graphite powder and 1.0 g of $NaNO_3$ were added into a 500 mL three-necked and round-bottomed flask with 50 mL of concentrated H_2SO_4 under vigorous stirring and ice bath. After stirring for 2 h, the stage addition of 6 g of $KMnO_4$ into the mixture was carried out in 2 h while the temperature was kept below 5 ℃. Then, the temperature of the above mixture was raised to 35 ℃ and the solution was kept vigorously stirred for 2 h. Subsequently, 80 mL of deionized water was added to the solution and the temperature of the mixture was heated to 98 ℃. After the slurry was stirred vigorously for another 1 h, 280 mL of deionized water and 80 mL of 30% H_2O_2 were added into the above mixture instantaneously to terminate the whole reaction. Finally, the mixture was cooled down to room temperature and centrifuged at 4000 rpm, washed with 5% aqueous HCl solution and water to remove the residual salts.

2.3. Preparation of CdS/rGO composite

CdS/rGO composite was prepared by the method reported previously[23] as following: 0.1589 g of cadmium acetate and 0.1583 g of thiourea (mole ratio: 1:3) were added into a 100 mL round-bottomed flask with 60 mL of deionized water to make a homogenous solution. Then, 20 mg of GO (the content of GO with respect to CdS is 20 wt.%) was added into the solution to form a homogeneous suspension with sonication. Finally, the mixture was transferred into a 100 mL Teflon-lined stainless steel autoclave and reacted under 180 ℃ for 12 h. The obtained products were centrifuged and washed extensively with deionized water and ethanol. The final product was obtained by lyophilization.

2.4. Preparation of CdS nanoparticles

CdS nanoparticles were synthesized for comparison following the same hydrothermal method with the preparation of CdS/rGO composite without the use of GO.

2.5. Preparation of rGO

rGO was synthesized for comparison following the same hydrothermal method as the preparation of CdS/rGO composite however without the use of cadmium acetate and thiourea.

2.6. Characterizations

Transmission electron microscopy (TEM) images of the samples were obtained using JEM-1400 microscopy (JEOL, Japan) to observe the morphologies of the materials. The crystal structures of all the samples were characterized by X-ray diffraction patterns (XRD, RigakuD/MAX 2550 diffractmeter) at room temperature. Raman spectra of the samples were recorded at room temperature using Raman microscopes (Renishaw, UK) under an excitation laser wavelength of 532 nm. UV/Vis absorption spectra were acquired with a scanning UV/Vis spectrophotometer (Varian, Cary 500). The X-ray photoelectron spectroscopy (XPS) data were recorded from a PerkinElmer PHI 500 ℃ ESCA system with a monochromatic Al Kα source operated at 250 W.

2.7. In situ generation of H_2O_2

In a typical experiment, 20 mg of CdS/rGO was dispersed in 20 mL of deionized water bubbled with O_2 for 30 min to obtain an O_2 equilibrated environment. Then, the suspension was stirred in dark for another 30 min to ensure adsorption-desorption equilibrium between the sample and reactant. Afterwards, the H_2O_2 production was conducted under a 300 W xenon lamp with a 420 nm cutoff filter to imitate visible light irradiation ($\lambda > 420$ nm) for 2 h. The concentration of H_2O_2 was determined by iodometric method with the addition of 2 mL of 0.1 M potassium iodide solution (KI) and 0.05 mL of 0.01 M ammonium molybdate solution ($H_8Mo_2N_2O_7$). The catalysts after photocatalytic generation of H_2O_2 were collected by centrifugation and washed with deionized water and ethanol.

2.8. Photo-Fenton degradation of phenol

In a typical experiment, 20 mg of CdS/rGO was dispersed in 20 mL of 10 mg/L phenol solution bubbled with O_2 for 30 min to obtain an O_2 equilibrated environment. To avoid Fe^{2+} being oxidized to Fe^{3+}, ferrous sulfate ($FeSO_4{\cdot}7H_2O$) was added after the O_2 bubbling. Then, the suspension was stirred in dark for another 30 min with 1.8 mM of $FeSO_4{\cdot}7H_2O$ to ensure adsorption-desorption equilibrium between the sample and reactant. Afterwards, the photo-Fenton reaction was conducted under a 300 W xenon lamp irradiation ($\lambda > 420$ nm) for 1 h. The concentration of phenol was investigated by a high-performance liquid chromatograph (HPLC) (Shimadzu SPD-M20 A). The catalysts after photocatalytic reaction were collected by centrifugation and washed with deionized water and ethanol. In the cycling experiments, new Fe^{2+} were added for each cycle.

3. Results and discussion

3.1. Characterization of the CdS/rGO composite

TEM images revealed that pure rGO was a partly wrinkled and folded 2D sheet (Fig. 1a) and CdS nanoparticles were predominantly spherical (Fig. 1b). With CdS nanoparticles plunged in, the rGO was highly wrinkled and folded (Fig. 1c). Meanwhile the CdS nanoparticles dispersed well on the rGO sheet, demonstrating the successful combination of CdS and rGO. The X-ray diffraction (XRD) patterns (Fig. 1d) of CdS, rGO and CdS/rGO composite exhibited the crystallographic phase of CdS and investigate the influence of graphene on the crystallinity of CdS nanoparticles. The strong peak at 26.4° corresponded to the diffraction of the (111) plane that can be assigned to hawleyite which was a cubic phase (JCPDS: 10-0454) of CdS. The weak peaks at 24.9°, 28.0°,

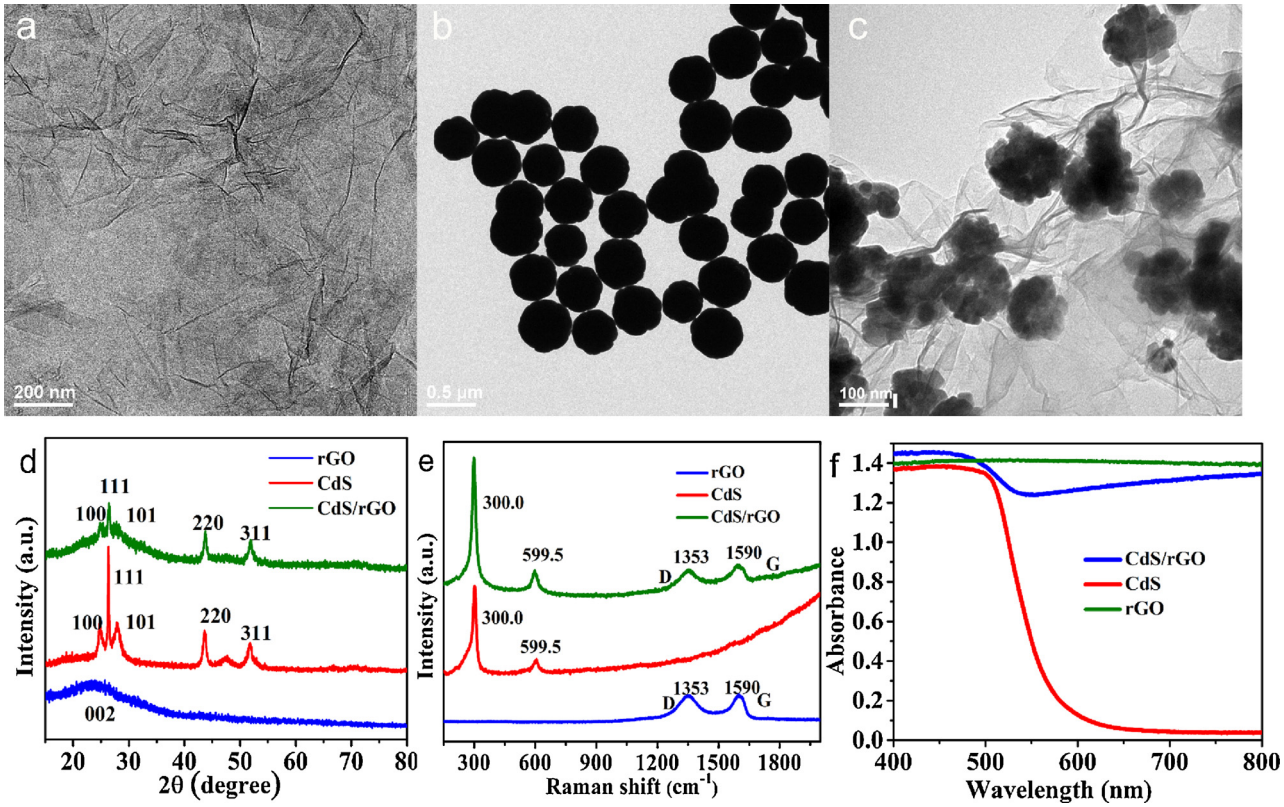

Fig. 1. (a–c) The TEM images of rGO, CdS and CdS/rGO; (d) XRD patterns and (e) Raman spectra of rGO, CdS and CdS/rGO; (f) UV–vis diffuse reflectance spectra of CdS, rGO and CdS/rGO.

43.8° and 52.0° corresponded to the diffractions of the (100), (101), (110) and (112) planes that can be ascribed to a hexagonal phase (JCPDS: 41-1049) of CdS [24,25]. The broad diffraction peak of rGO was shown at 24° [23]. No other typical diffraction peaks had been found in CdS/rGO, which meant that the hydrothermal process had not changed the chemical constitution and crystallinity.

The Raman spectra of CdS, rGO and CdS/rGO were displayed in Fig. 1e. The spectrum of CdS/rGO simultaneously possesses the typical peaks of rGO at 1590 cm^{-1} and 1353 cm^{-1} for the G-band and D-band and the peaks for CdS at about 300.0 cm^{-1} and 599.5 cm^{-1}, further proving the successful preparation of the CdS/rGO composite [23,26].

The optical properties of samples were investigated by UV–vis diffuse reflectance spectroscopy (Fig. 1f). Bare CdS nanoparticles absorbed light with wavelengths shorter than ~550 nm, indicating a relatively little usage of the visible light because of their small intrinsic band gap. After the hydrothermal process with GO, the light absorption edge shifted towards longer wavelengths, which means CdS/rGO composites can utilize more visible light to enhance photocatalytic activity because of the ability of rGo to absorb visible light.

3.2. Photo-Fenton degradation of phenol

In this work, the photo-Fenton system was constructed by CdS/rGO and Fe^{2+}, in which CdS/rGO was responsible for the *in situ* generation of H_2O_2 by photocatalysis. The ability of CdS/rGO to generate H_2O_2 was first evaluated in the absence of Fe^{2+}. The experiment was conducted under visible light irradiation ($\lambda > 420$ nm, Xe lamp) in O_2-saturated deionized water at room temperature. The result is shown in Fig. 2a. A H_2O_2 production of 580.68 μmol/L was achieved by the CdS/rGO composite in 2 h of reaction. For comparison, the productions of H_2O_2 from bare rGO and bare CdS were also tested. Bare rGO produced no H_2O_2 (0 μmol/L) and bare CdS produced 85.58 μmol/L of H_2O_2, demonstrating that the CdS/rGO composite produced much more H_2O_2 than bare rGO or bare CdS. The combination of CdS and rGO increased the production of H_2O_2 because the photo-excited e^- in the conduction band of CdS could be transferred from CdS to rGO which efficiently promoted the charge separation and consequently improved the photocatalytic activity for the generation of H_2O_2 [23].

Fe^{2+} was then added to the suspension of CdS/rGO. With the presence of Fe^{2+}, a photo-Fenton system with H_2O_2 *in situ* generated by CdS/rGO under visible light irradiation was constructed. Subsequently, the ability of the system to degrade organic pollutants represented by phenol was investigated. The experiments were carried out at natural pH without adjustment. The results are shown in Fig. 2b. C_0 is the initial concentration of phenol and C is the concentration of phenol after the photo-Fenton degradation. It can be found that a complete phenol removal was achieved in 60 min of treatment by the CdS/rGO/Fe^{2+} system. Under the same conditions, only about 45% of phenol was degraded by CdS/Fe^{2+}, because CdS produced much less H_2O_2 than CdS/rGO as shown in Fig. 2a. rGO /Fe^{2+} removed only about 18% of phenol mainly as a result of the rGO's absorption capability. For comparison, photo-Fenton degradation of phenol with typical TiO_2 photocatalyst instead of CdS/rGO was conducted. The result is shown in Fig. S1, which tells that TiO_2 has no activity in this system.

Generally, the degradation efficiency of organic pollutants in Fenton process is influenced by the concentration of Fe^{2+} ions since Fe^{2+} is a crucial reagent [27]. Therefore, degradation experiments with different Fe^{2+} concentrations of 0.9, 1.8 and 2.7 μM were carried out at room temperature and natural pH. Results are presented in Fig. 2c. With increasing Fe^{2+} concentration from 0.9 μM to 1.8 μM, the degradation rate of phenol increases. However, further increase in the concentration of Fe^{2+} led to a decrease in the degradation. The reason is that the excessive Fe^{2+} concentration can be oxidized by $^{\cdot}OH$ to generate Fe^{3+} and HO^- (Eq. (3)) [28–30]. Therefore, 1.8 μM was selected as an optimal Fe^{2+} concentration for the following studies.

$$Fe^{2+} + HO^{\cdot} \rightarrow Fe^{3+} + HO^- \quad (3)$$

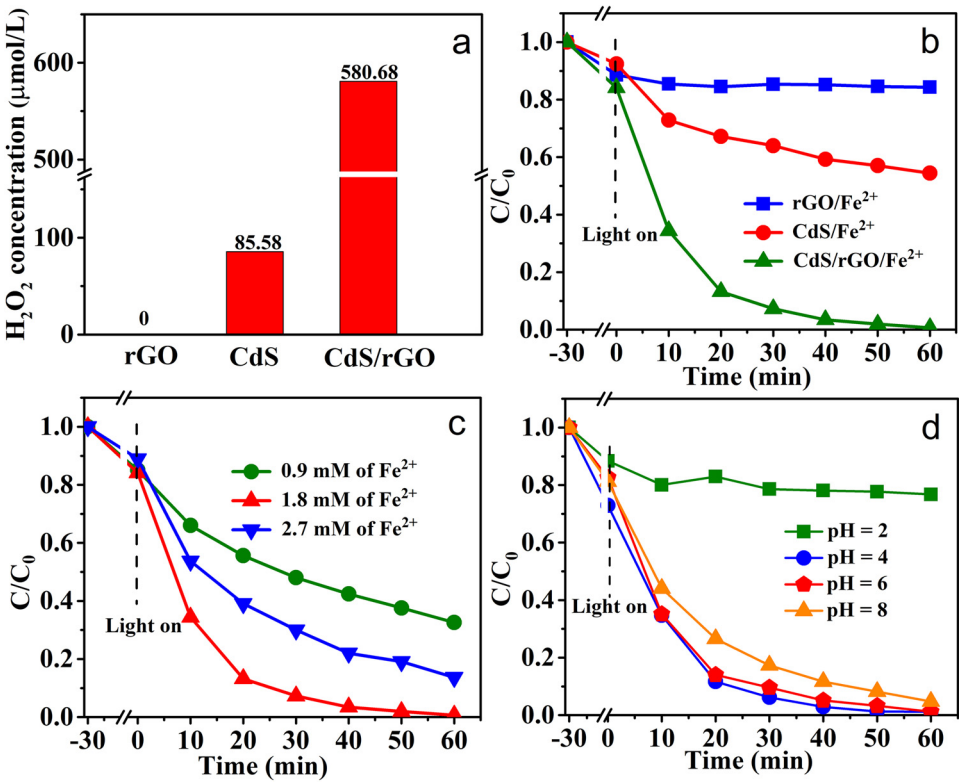

Fig. 2. (a) *In situ* generation of H_2O_2 by using rGO, CdS and CdS/rGO; (b) Photo-Fenton degradation of phenol with *in situ*-generated H_2O_2 by using rGO/Fe^{2+}, CdS/Fe^{2+} and CdS/rGO/Fe^{2+}; (c) Effect of Fe^{2+} concentration on the degradation of phenol for CdS/rGO/Fe^{2+} system; (d) The influence of different pH for the phenol degradation by using *in situ*-generated H_2O_2.

In addition, the effect of pH on Fenton reaction is necessary to be investigated. It is well known that the photo-Fenton reaction is strongly dependent on the solution's pH, and the optimum pH is generally around 3 [31]. However, if the catalysts contain GO, it can overcome the sensitivity of the process to pH due to the high functional groups of GO [32]. The reaction was first conducted at natural pH, which was tested to be about 6 without adjustment. Afterwards, experiments for comparison were carried out, in which pH was adjusted to be at 4 and 2 using HCl aqueous solution (0.1 mol/L) and adjusted to be at 8 using NaOH aqueous solution (1 mol/L). From Fig. 2d, it was observed that phenol almost could not be degraded when the pH value reached 2, which was probably because CdS in the composite catalyst reacted with HCl under strong acidic condition, leading to a great decrease in the production of H_2O_2. The system demonstrated good degradation activity from pH = 4 to pH = 6. When the pH reached 8, the degradation activity slightly decreased but still works efficiently. Therefore, this system can work well from pH = 4 to pH = 8 and it doesn't extra cost for adjusting pH value.

The recyclic experiments were performed to study the stability of the catalyst and photo-Fenton system. The experiments were divided into two parts. First, the photocatalytic generation of H_2O_2 was repeated for up to five cycles under the same condition (Fig. 3a). After five test cycles, there was almost no change in the production of H_2O_2, suggesting that the CdS/rGO composite catalyst can be stable and reusable. Then the photo-Fenton degradation of phenol using *in situ* generated H_2O_2 was repeated for five times and phenol almost degraded completely every time (Fig. 3b). In addition, the morphology and the XRD pattern of the phohocatalyst remains almost the same after the cyclic reaction (Figs. 3c and S2). Finally, Total Organic Carbon (TOC) was measured to investigate the mineralization degree of phenol in the photo-Fenton system. The results shown in Fig. 3d indicate a mineralization degree of 43.66% was achieved using the CdS/rGO/Fe^{2+} system in 1 h, which was relatively higher than that reported in relevant literature [15], demonstrating that the photo-Fenton system with *in situ* generated H_2O_2 constructed in this work performs efficiently and consistently.

3.3. Possible mechanism for the photo-Fenton degradation with in situ-generated H_2O_2

The mechanism was investigated from two aspects. One was the mechanism of the generation of H_2O_2 and the other was the photo-Fenton degradation of phenol. The generation of H_2O_2 has been reported to be a process of photocatalytic reduction of O_2 [33]. It is well known that there are two routes to generate H_2O_2 by reducing O_2: a two-electron on- step direct reduction route (Eq. (4)) and a sequential single-electron two-step indirect reduction route (Eqs. (5) and (6)) [34,35].

$$O_2 + 2H^+ + 2e^- \rightarrow H_2O_2 \quad (4)$$

$$O_2 + e^- \rightarrow {}^{\cdot}O_2^- \quad (5)$$

$${}^{\cdot}O_2^- + 2H^+ + e\text{-} \rightarrow H_2O_2 \quad (6)$$

In order to clarify the mechanisms of the generation of H_2O_2, DMPO spin-trapping ESR technique was employed to measure whether the ${}^{\cdot}O_2^-$ had been generated during the process or not. The characteristic signals of ${}^{\cdot}O_2$- in Fig. 4a are in align with the reported values [36] and different from that measured before the light irradiation (Fig. S3), confirming the formation of ${}^{\cdot}O_2^-$ in the photocatalytic generation process of H_2O_2. However, the intensity of the signals is so weak that the generation of ${}^{\cdot}O_2^-$ can be seen as pure minority. Based on the above results, it implies that a two-electron one-step reduction route might dominate the whole H_2O_2 production process but the sequential single-electron two-step reduction route also exist. This electron reduction mechanism conforms with the reported literature [23]. To test above hypothesis, active species trapping experiment was further conducted. As shown in Fig. 4b, with the addition of p-benzoquinone (PBQ, 1 mM) to scavenge ${}^{\cdot}O_2^-$ [37–40], the photo-Fenton degradation of phenol was decreased to 83.4%. It implies that ${}^{\cdot}O_2^-$ had effect on the formation of H_2O_2 and consequently affected the degradation of phenol but the influence was not significant [41]. Therefore, it can unambiguously prove that the *in situ* generation of H_2O_2 pathway under visible light was a dominant two-electron one-step reduction with the

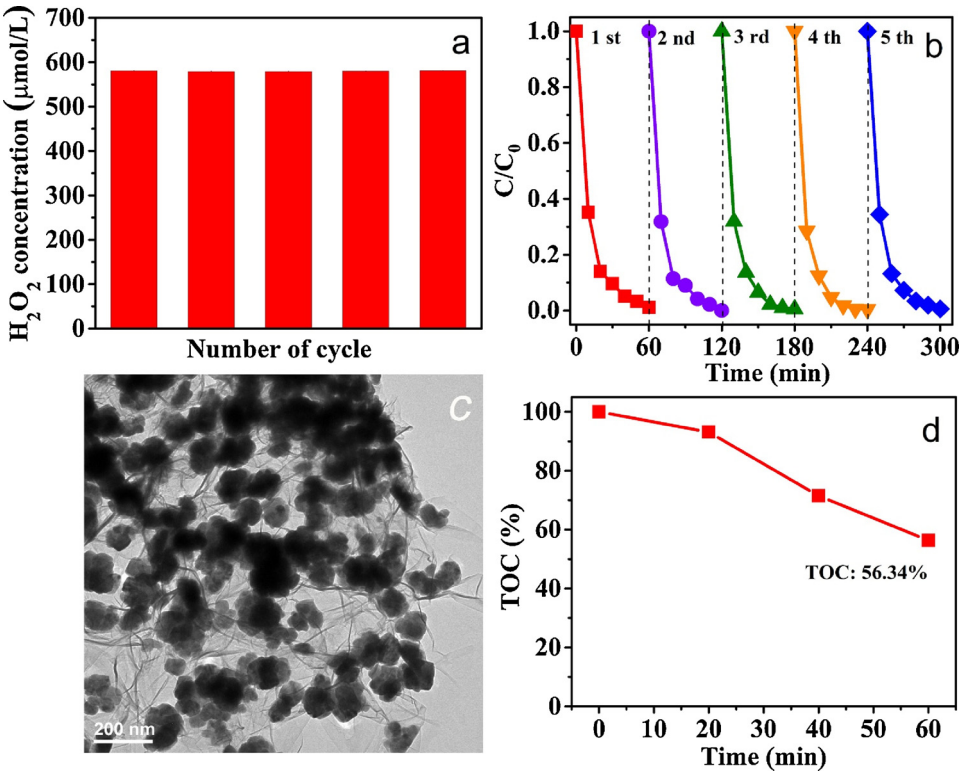

Fig. 3. Recyclability study of (a) *in situ* generation of H_2O_2; (b) the photo-Fenton degradation of phenol with *in situ*-generated H_2O_2 at natural pH; (c) the TEM images of CdS/rGO after five repeated experiments. (d) TOC conversions during phenol degradation with *in situ*-generated H_2O_2 at natural pH.

assistance of a sequential single-electron two-step reduction route.

Subsequently, several control experiments were conducted to reveal the mechanism for the photo-Fenton degradation. First, the degradation efficiency of CdS/rGO with and without Fe^{2+} were compared. It can be observed from Fig. 5a that, when there were no Fe^{2+} in the system, negligible phenol was degraded, proving that the degradation of phenol was a result of the interaction between Fe^{2+} and *in situ* generated H_2O_2. Without Fe^{2+}, the H_2O_2 generated by CdS/rGO cannot be decomposed to form hydroxyl radicals for oxidation of phenol. This result also excludes the possibility that the degradation of phenol was due to the photocatalytic degradation of CdS/rGO. Second, because the generation of H_2O_2 comes from the reduction of O_2, the degradation efficiency under O_2 atmosphere and N_2 atmosphere were also compared for the CdS/rGO/Fe^{2+} system. Fig. 5a shows that there was much less degradation of phenol under N_2 atmosphere than that under O_2 atmosphere. Under N_2 atmosphere, only little O_2 adsorbed on the catalyst can contribute to the formation of H_2O_2. Therefore, without sufficient O_2, little H_2O_2 could be generated to react with Fe^{2+} for the formation of hydroxyl radicals and consequently the degradation of phenol greatly decreased. Last, the degradation efficiency in the presence of Fe^{2+} with and without CdS/rGO were compared, the result is shown in Fig. 5b. Obviously, almost no phenol was degraded when there was no CdS/rGO in the system. This result excludes the possibility that the removal of phenol was caused by the flocculation of iron or ferrous ions. Overall, the above results all prove that efficient degradation of phenol comes from the interaction of Fe^{2+} and *in situ* generated H_2O_2 by CdS/rGO.

The PL technique has been proven to be useful in detecting radical species [42], providing essential information for understanding the reaction mechanisms. It has been reported that benzoic acid (BA) can scavenge ·OH radicals to form the fluorescent compound, hydroxybenzoic acid (HBA) [43]. Because ·OH radicals are the main species to oxidize organic pollutants in photo-Fenton process, we took advantage

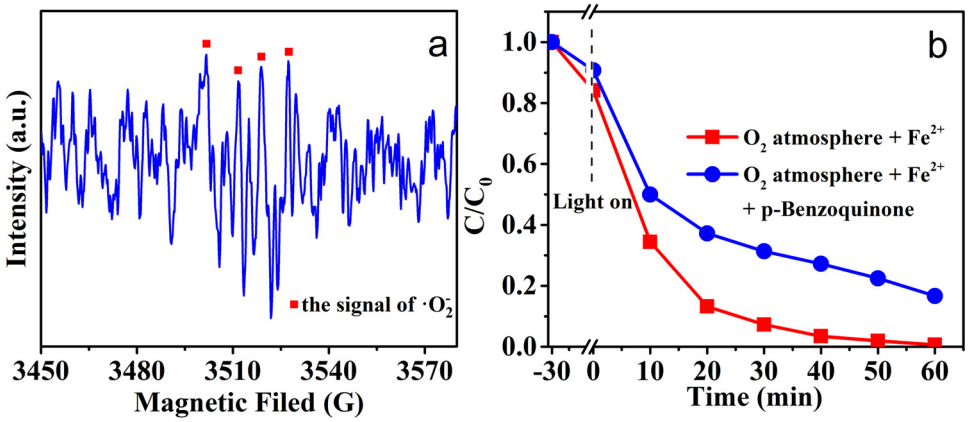

Fig. 4. a) 5,5-dimethyl-pyrroline N-oxide (DMPO) spin trapping ESR technique to measure $^{\cdot}O_2^-$ generated during the *in situ* generation of H_2O_2; b) the influence of p-benzoquinone (PBQ, 1 mM, $^{\cdot}O_2^-$ scavenger) for the phenol degradation.

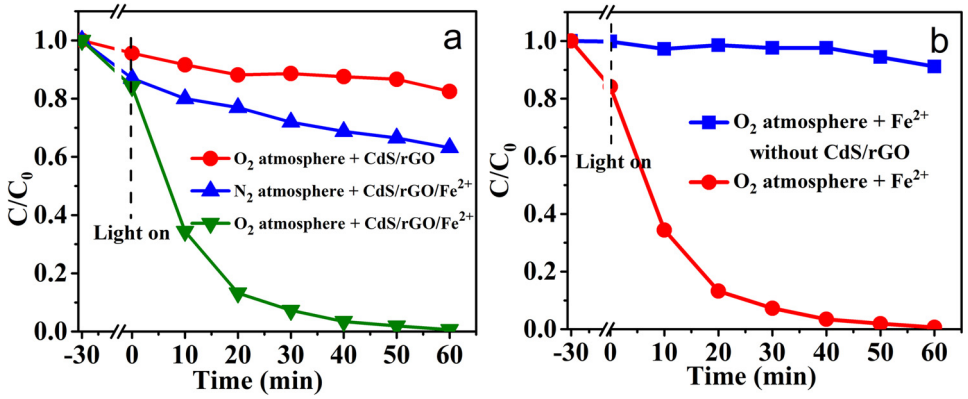

Fig. 5. a) Phenol degradation with the usage of CdS/rGO under different conditions; b) Phenol degradation in the presence of Fe^{2+} with and without CdS/rGO.

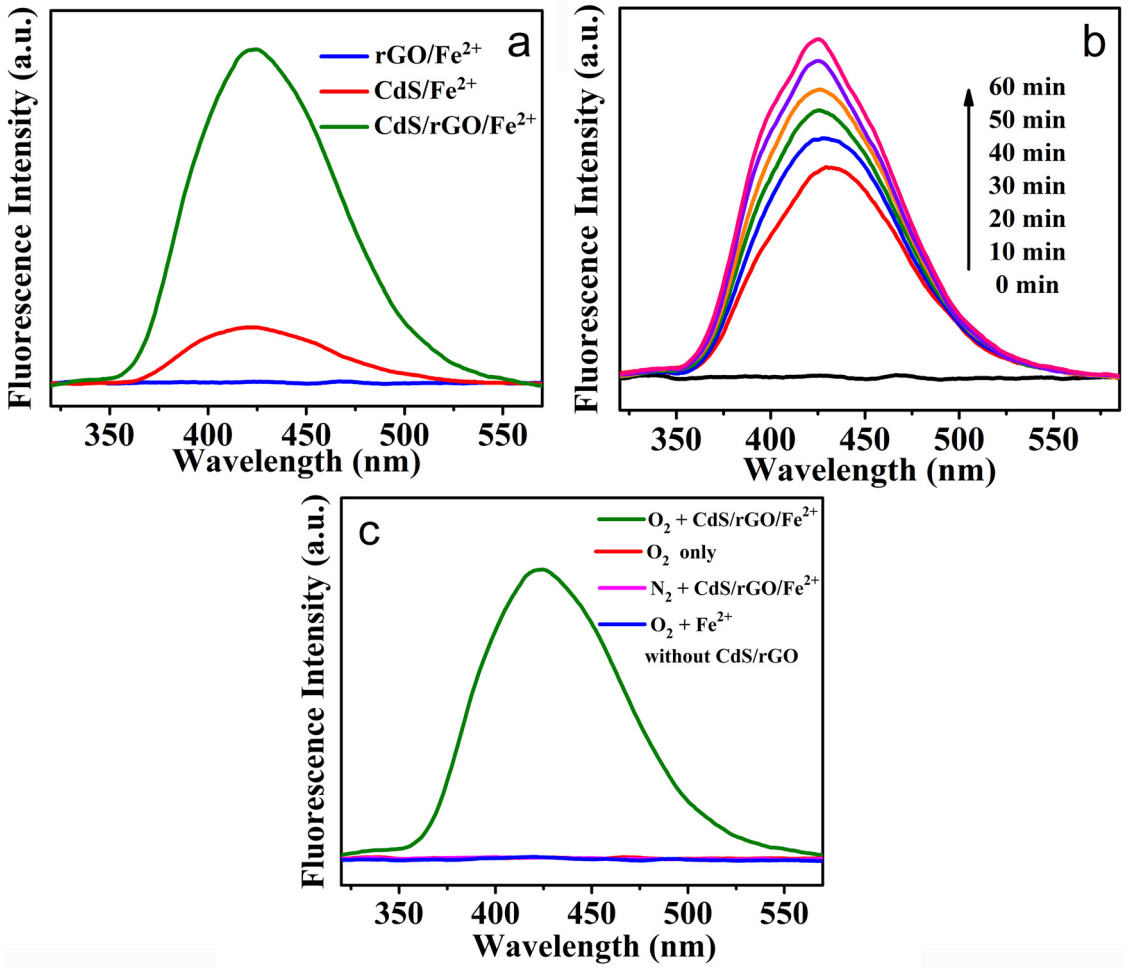

Fig. 6. a) PL spectra of rGO/Fe^{2+}, CdS/Fe^{2+} and $CdS/rGO/Fe^{2+}$ system under visible light irradiation in O_2-saturated solution; b) PL spectra of $CdS/rGO/Fe^{2+}$ system at different reaction time; c) PL spectra under different conditions with visible light irradiation.

of this benzoic acid reaction to further reveal the reactivity and reaction pathway of the $CdS/rGO/Fe^{2+}$ system using PL spectroscopy. Fig. 6a shows different PL intensity with different system under visible light irradiation in O_2-saturated solution. Usually, the PL intensity is proportional to the amount of ˙OH radicals produced [42]. As seen in Fig. 6a, the $CdS/rGO/Fe^{2+}$ system showed much higher PL intensity than CdS/Fe^{2+} and rGO/Fe^{2+}, indicating that the $CdS/rGO/Fe^{2+}$ system produced much more ˙OH radicals. This tendency is in agreement with their photo-Fenton degradation of phenol shown in Fig. 2b. Then, the PL intensities for the $CdS/rGO/Fe^{2+}$ system at different irradiation time were investigated (Fig. 6b). There was a gradual increase of the PL intensity as irradiation time increased, demonstrating substantial ˙OH radicals were generated by the system for the oxidation of phenol. Fig. 6c presents the PL spectra under different conditions. From the figure, it can be found that: (1) when there were no CdS/rGO and Fe^{2+} in the system, no ˙OH radicals were produced; (2) the alone existence of Fe^{2+} without CdS/rGO could not produce ˙OH radicals; (3) without O_2 in the system, no ˙OH radicals could be detected although CdS/rGO and Fe^{2+} were both present. Collectively, it demonstrates that the ˙OH radicals could only be produced abundantly with the

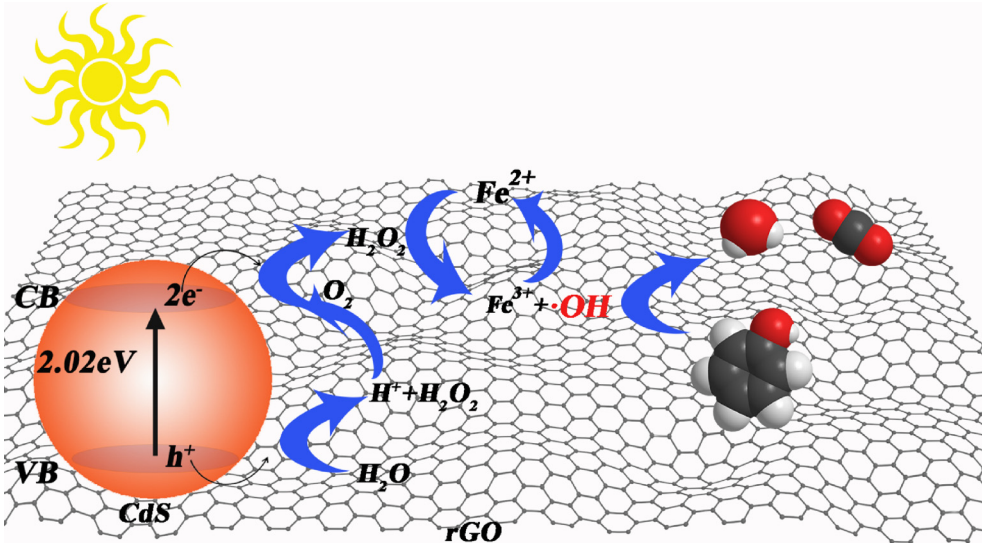

Fig. 7. A plausible mechanism proposed for the photo-Fenton degradation of phenol with *in situ*-generated H_2O_2.

simultaneous existence of CdS/rGO, Fe^{2+} and O_2.

On the basis of the above results, a plausible mechanism of the CdS/rGO/Fe^{2+} photo-Fenton system with *in situ* generated H_2O_2 for the degradation of phenol is proposed in Fig. 7. First, the photo-generated electrons from CdS can transfer to rGO and then take part in the reduction reaction of O_2 to generate H_2O_2. On the other hand, the holes on the valence band oxidizes water [23], occurring reactions as shown in Eqs. (7) and (8) [44,45],

$$H_2O + h^+ \rightarrow H^+ + {}^{\cdot}OH \quad (7)$$

$$2\,{}^{\cdot}OH \rightarrow H_2O_2 \quad (8)$$

${}^{\cdot}OH$ and H^+ were produced, then the 2 ${}^{\cdot}OH$ combine to form H_2O_2. Subsequently, the Fe^{2+} reacted with the *in situ* generated H_2O_2 to form abundant ${}^{\cdot}OH$ radicals which efficiently oxidize the organic pollutants.

4. Conclusion

In this work, a photo-Fenton system of CdS/rGO/Fe^{2+} with *in situ*-generated H_2O_2 was constructed. In this system, CdS/rGO was able to produce H_2O_2 under visible light irradiation with a rate of 580.68 μmol/L, which could be utilized in time by Fe^{2+} to form abundant hydroxyl radicals. Consequently, organic pollutants represented by phenol could be efficiently degraded by the strong oxidizing hydroxyl radicals. A TOC removal efficiency of 43.66% was achieved in 1 h for the degradation of phenol. In addition, this photo-Fenton degradation of phenol was performed efficiently and stably at natural pH without pH adjustment. We anticipate the results presented here provide new insights into rational fabrication of photo-Fenton systems towards sustainable wastewater treatment.

Conflict of interest

The authors declare no competing financial interest.

Acknowledgments

This work was financially supported by National Nature Science Foundation of China (21777044, 21677048, 5171101651), the State Key Research Development Program of China (2016YFA0204200), the Science and Technology Commission of Shanghai Municipality (16JC1401400, 17520711500), Fundamental Research Funds for the Central Universities (222201714061, 222201817009, 22221815006, 22221818014).

Appendix A. Supplementary data

Supplementary material related to this article can be found, in the online version, at doi:https://doi.org/10.1016/j.apcatb.2018.09.049.

References

[1] P. Villegas- Guzman, S. Giannakis, S. Rtimi, D. Grandjean, M. Bensimon, L.F. de Alencastro, R. Torres-Palma, C. Pulgarin, A green solar photo-Fenton process for the elimination of bacteria and micropollutants in municipal wastewater treatment using mineral iron and natural organic acids, Appl. Catal. B: Environ. 219 (2017) 538–549.

[2] N. Klamerth, S. Malato, M.I. Maldonado, A. Agüera, A.R. Fernández-Alba, Application of Photo-Fenton as a tertiary treatment of emerging contaminants in municipal wastewater, Environ. Sci. Technol. 44 (2010) 1792–1798.

[3] W. Zhao, C. Liang, B. Wang, S. Xing, Enhanced Photocatalytic and Fenton-like Performance of CuO_x-Decorated $ZnFe_2O_4$, ACS Appl. Mater. Interfaces 9 (2017) 41927–41936.

[4] I. Carra, S. Malato, M. Jiménez, M.I. Maldonado, J.A. Sánchez Pérez, Microcontaminant removal by solar photo-Fenton at natural pH run with sequential and continuous iron additions, Chem. Eng. J. 235 (2014) 132–140.

[5] R.F. Hems, J.S. Hsieh, M.A. Slodki, S. Zhou, J.P.D. Abbatt, Suppression of OH generation from the Photo-Fenton reaction in the presence of α-pinene secondary organic aerosol material, Environ. Sci. Technol. Lett. 4 (2017) 439–443.

[6] T.M. Do, J.Y. Byun, S.H. Kim, Magnetite-coated metal foams as one-body catalysts for Fenton-like reactions, Res. Chem. Intermed. 43 (2016) 3481–3492.

[7] R.G. Zepp, B.C. Faust, J. Hoigne, Hydroxyl radical formation in aqueous reactions (pH 3-8) of iron(II) with hydrogen peroxide: the photo-Fenton reaction, Environ.Sci.Technol 26 (1992) 313–319.

[8] X. Zhou, Y. Zhang, C. Wang, X. Wu, Y. Yang, B. Zheng, H. Wu, S. Guo, J. Zhang, Photo-Fenton reaction of graphene oxide: a new strategy to prepare graphene quantum dots for DNA cleavage, ACS Nano 6 (2012) 6592–6599.

[9] X. Yan, K. Gan, B. Tian, J. Zhang, L. Wang, D. Lu, Photo-Fenton refreshable Fe_3O_4@HCS adsorbent for the elimination of tetracycline hydrochloride, Res. Chem. Intermed. 44 (2017) 1–11.

[10] L. Clarizia, D. Russo, I. Di Somma, R. Marotta, R. Andreozzi, Homogeneous photo-Fenton processes at near neutral pH: a review, Appl. Catal. B 209 (2017) 358–371.

[11] W. Shi, D. Du, B. Shen, C. Cui, L. Lu, L. Wang, J. Zhang, Synthesis of yolk–shell structured Fe_3O_4@void@CdS nanoparticles: a general and effective structure design for photo-Fenton reaction, ACS Appl. Mater. Interfaces 8 (2016) 20831–20838.

[12] S. Tian, J. Zhang, J. Chen, L. Kong, J. Lu, F. Ding, Y. Xiong, $Fe_2(MoO_4)_3$ as an effective photo-Fenton-like catalyst for the degradation of anionic and cationic dyes in a wide pH range, Ind. Eng. Chem. Res. 52 (2013) 13333–13341.

[13] Y. Liu, Q. Fan, J. Wang, Zn-Fe-CNTs catalytic in situ generation of H_2O_2 for Fenton-like degradation of sulfamethoxazole, J. Hazard. Mater. 342 (2018) 166–176.

[14] B. Puértolas, A.K. Hill, T. García, B. Solsona, L. Torrente-Murciano, In-situ synthesis of hydrogen peroxide in tandem with selective oxidation reactions: a mini-review, Catal. Today 248 (2015) 115–127.

[15] M.S. Yalfani, S. Contreras, F. Medina, J.E. Sueiras, Hydrogen substitutes for the in situ generation of H_2O_2: an application in the Fenton reaction, J. Hazard. Mater. 192 (2011) 340–346.

[16] Y. Shiraishi, S. Kanazawa, Y. Sugano, D. Tsukamoto, H. Sakamoto, S. Ichikawa, T. Hirai, Highly selective production of hydrogen peroxide on graphitic carbon nitride (g-C_3N_4) photocatalyst activated by visible light, ACS Catal. 4 (2014) 774–780.

[17] A. Mehri, H. Kochkar, In situ generated H_2O_2over supported Pd–Au clusters in hybrid titania nanocrystallites, Chem. Lett. 43 (2014) 1046–1048.
[18] A. Asghar, A.A. Abdul Raman, W.M.A. Wan Daud, Advanced oxidation processes for in-situ production of hydrogen peroxide/hydroxyl radical for textile wastewater treatment: a review, J. Clean. Prod. 87 (2015) 826–838.
[19] D. Tsukamoto, A. Shiro, Y. Shiraishi, Y. Sugano, S. Ichikawa, S. Tanaka, T. Hirai, Photocatalytic H2O2 production from ethanol/O2 system using TiO2 loaded with Au–Ag bimetallic alloy nanoparticles, ACS Catal. 2 (2012) 599–603.
[20] M.S. Yalfani, S. Contreras, F. Medina, J. Sueiras, Phenol degradation by Fenton's process using catalytic in situ generated hydrogen peroxide, Appl. Catal. B 89 (2009) 519–526.
[21] G.H. Moon, S. Kim, Y.J. Cho, J. Lim, D.H. Kim, W. Choi, Synergistic combination of bandgap-modified carbon nitride and WO_3 for visible light-induced oxidation of arsenite accelerated by in-situ Fenton reaction, Appl. Catal. B 218 (2017) 819–824.
[22] B. Qiu, Y. Deng, Q. Li, B. Shen, M. Xing, J. Zhang, Rational design of a unique ternary structure for highly photocatalytic nitrobenzene reduction, J. Phys. Chem. C 120 (2016) 12125–12131.
[23] S. Thakur, T. Kshetri, N.H. Kim, J.H. Lee, Sunlight-driven sustainable production of hydrogen peroxide using a CdS–graphene hybrid photocatalyst, J. Catal. 345 (2017) 78–86.
[24] J. Wang, S. Liang, L. Ma, S. Ding, X. Yu, L. Zhou, Q. Wang, One-pot synthesis of CdS–reduced graphene oxide 3D composites with enhanced photocatalytic properties, CrystEngComm 16 (2014) 399–405.
[25] Y. Liu, P. Zhang, B. Tian, J. Zhang, Core–shell structural CdS@SnO_2 nanorods with excellent visible-light photocatalytic activity for the selective oxidation of benzyl alcohol to benzaldehyde, ACS Appl. Mater. Interfaces 7 (2015) 13849–13858.
[26] K. Krishnamoorthy, M. Veerapandian, R. Mohan, S.-J. Kim, Investigation of Raman and photoluminescence studies of reduced graphene oxide sheets, Appl. Phys. A 106 (2011) 501–506.
[27] G.M.S. ElShafei, F.Z. Yehia, O.I.H. Dimitry, A.M. Badawi, G. Eshaq, Degradation of nitrobenzene at near neutral pH using Fe^{2+}–glutamate complex as a homogeneous Fenton catalyst, Appl. Catal. B 99 (2010) 242–247.
[28] E. Brillas, I. Sirés, M.A. Oturan, Electro-fenton process and related electrochemical technologies based on Fenton's reaction chemistry, Chem. Rev. 109 (2009) 6570–6631.
[29] M. Sedaghat, B. Vahid, S. Aber, M.H. Rasoulifard, A. Khataee, N. Daneshvar, Electrochemical and photo-assisted electrochemical treatment of the pesticide imidacloprid in aqueous solution by the Fenton process: effect of operational parameters, Res. Chem. Intermed. 42 (2015) 855–868.
[30] L. Zhou, J. Lei, L. Wang, Y. Liu, J. Zhang, Highly efficient photo-Fenton degradation of methyl orange facilitated by slow light effect and hierarchical porous structure of Fe_2O_3 -SiO_2 photonic crystals, Appl. Catal. B 237 (2018) 1160–1167.
[31] T. Xu, R. Zhu, G. Zhu, J. Zhu, X. Liang, Y. Zhu, H. He, Mechanisms for the enhanced photo-Fenton activity of ferrihydrite modified with $BiVO_4$ at neutral pH, Appl. Catal. B 212 (2017) 50–58.
[32] Y.-C. Lee, S.-J. Chang, M.-H. Choi, T.-J. Jeon, T. Ryu, Y.S. Huh, Self-assembled graphene oxide with organo-building blocks of Fe-aminoclay for heterogeneous Fenton-like reaction at near-neutral pH: a batch experiment, Appl. Catal. B 142-143 (2013) 494–503.
[33] Y. Kofuji, Y. Isobe, Y. Shiraishi, H. Sakamoto, S. Tanaka, S. Ichikawa, T. Hirai, Carbon nitride-aromatic diimide-graphene nanohybrids: metal-free photocatalysts for solar-to-hydrogen peroxide energy conversion with 0.2% efficiency, J. Am. Chem. Soc. 138 (2016) 10019–10025.
[34] J. Wang, K. Chen, Y. Shen, X. Wang, Y. Guo, X. Zhou, R. Bai, Enhanced photocatalytic degradation for organic pollutants by a novel m-Bi_2O_4/$Bi_2O_2CO_3$ photocatalyst under visible light, Res. Chem. Intermed. 44 (2018) 3061–3079.
[35] Y. Peng, L. Wang, Y. Liu, H. Chen, J. Lei, J. Zhang, Visible-light-driven photocatalytic h_2o_2 production on g-$c_3n_4$loaded with cop as a noble metal free cocatalyst, Eur. J. Inorg. Chem. 2017 (2017) 4797–4802.
[36] S. Li, G. Dong, R. Hailili, L. Yang, Y. Li, F. Wang, Y. Zeng, C. Wang, Effective photocatalytic H_2O_2 production under visible light irradiation at g-C_3N_4 modulated by carbon vacancies, Appl. Catal. B 190 (2016) 26–35.
[37] H. Huang, Y. He, X. Du, P.K. Chu, Y. Zhang, A general and facile approach to heterostructured Core/Shell $BiVO_4$/BiOI p–n junction: room-temperature in situ assembly and highly boosted visible-light photocatalysis, ACS Sustain. Chem. Eng. (3) (2015) 3262–3273.
[38] J. Lei, F. Liu, L. Wang, Y. Liu, J. Zhang, A binary polymer composite of graphitic carbon nitride and poly(diphenylbutadiyne) with enhanced visible light photocatalytic activity, RSC Adv. 7 (2017) 27377–27383.
[39] L. Zhou, Y. Tian, J. Lei, L. Wang, Y. Liu, J. Zhang, Self-modification of g-C_3N_4 with its quantum dots for enhanced photocatalytic activity, Catal. Sci. Technol. 8 (2018) 2617–2623.
[40] F. Liu, J. Yu, G. Tu, L. Qu, J. Xiao, Y. Liu, L. Wang, J. Lei, J. Zhang, Carbon nitride coupled Ti-SBA15 catalyst for visible-light-driven photocatalytic reduction of Cr (VI) and the synergistic oxidation of phenol, Appl. Catal. B 201 (2017) 1–11.
[41] J. Xiao, Y. Xie, Q. Han, H. Cao, Y. Wang, F. Nawaz, F. Duan, Superoxide radical-mediated photocatalytic oxidation of phenolic compounds over Ag(+)/TiO(2): Influence of electron donating and withdrawing substituents, J. Hazard. Mater. 304 (2016) 126–133.
[42] J. Yu, G. Dai, B. Cheng, Effect of crystallization methods on morphology and photocatalytic activity of anodized TiO2 nanotube array films, J. Phys. Chem. C 114 (2010) 19378–19385.
[43] M. Xing, J. Zhang, B. Qiu, B. Tian, M. Anpo, M. Che, A brown mesoporous TiO_{2-x}/MCF composite with an extremely high quantum yield of solar energy photocatalysis for H_2 evolution, Small 11 (2015) 1920–1929.
[44] V. Diesen, M. Jonsson, Formation of H_2O_2 in TiO_2 photocatalysis of oxygenated and deoxygenated aqueous systems: a probe for photocatalytically produced hydroxyl radicals, J. Phys. Chem. C 118 (2014) 10083–10087.
[45] H. Zhuang, L. Yang, J. Xu, F. Li, Z. Zhang, H. Lin, J. Long, X. Wang, Robust photocatalytic H_2O_2 production by octahedral $Cd_3(C_3N_3S_3)_2$ coordination polymer under visible light, Sci. Rep. 5 (16947) (2015) 1–8.